Chemical Science

Accepted Manuscript

View Article Online
DOI: 10.1039/C9SC05404A

ARTICLE

The Synthesis of Brominated-Boron-Doped PAHs by Alkyne 1,1-Bromoboration: Mechanistic and Functionalisation Studies

Received 00th January 20xx,
Accepted 00th January 20xx

DOI: 10.1039/x0xx00000x

K. Yuan[a], R. J. Kahan[b], C. Si[c], A. Williams[b], S. Kirschner[a], M. Uzelac[a], E. Zysman-Colman*[c] and M. J. Ingleson[a]*

The synthesis of a range of brominated-B_n-containing (n = 1, 2) polycyclic aromatic hydrocarbons (PAHs) is achieved simply by reacting BBr_3 with appropriately substituted alkynes via a bromoboration/electrophilic C-H borylation sequence. The brominated-B_n-PAHs were isolated as either the borinic acid or B-mesityl-protected derivatives, with the latter having extremely deep LUMOs for the B_2-doped PAHs (with one example having a reduction potential of $E_{1/2}$ = -0.96 V versus Fc^+/Fc, Fc = ferrocene). Mechanistic studies revealed the reaction sequence proceeds by initial alkyne 1,1-bromoboration. 1,1-bromoboration also was applied to access a number of unprecedented 1-bromo-2,2-diaryl substituted vinylboronate esters direct from internal alkynes. Bromoboration/C-H borylation installs useful C-Br units onto the B_n-PAHs, which were utilised in Negishi coupling reactions, including for the installation of two triarylamine donor (D) groups onto a B_2-PAH. The resultant D-A-D molecule has a low optical gap with an absorption onset at 750 nm and emission centered at 810 nm in the solid state.

Introduction

The incorporation of main group elements into conjugated organic scaffolds is a powerful strategy to tune electronic properties.[1] Recently, this approach has been extended to the introduction of three-coordinate boron atoms into polycyclic aromatic hydrocarbons (PAHs).[1,2] In these "B-doped"-PAHs interaction between the empty p orbital on boron and the extended π system often leads to molecules with low energy LUMOs.[2] B-doped PAHs now are being explored for a range of applications including organic light-emitting diodes, thin film transistors, solar cells, lithium batteries and electrocatalysis.[2] However, two factors have limited the wider uptake of purely B-doped PAHs (i.e. PAHs without co-doping elements e.g. N): (i) the limited simple synthetic routes to form B_n-PAHs, particularly for n > 1, which generally have the deeper LUMOs;[2] (ii) the challenge associated with incorporating B_n-doped-PAHs into more complex materials, e.g. by coupling reactions to access donor-acceptor (D-A) structures.[3] Some notable progress has been made addressing (i), with several routes to larger B_n-PAHs, (n ≥ 2, see **A** – **D**, Figure 1) including examples with low LUMO energies, recently reported.[4,5] However, the incorporation of B_n-PAHs into more complex materials currently requires the post synthetic introduction of additional functionality onto the B_n-PAH to enable subsequent steps (e.g. cross coupling).[6] This has associated challenges (e.g. selectivity in halogenation) along with step-economy issues. Therefore, a simple route to form a range of B_n-doped PAHs with low LUMO energies that concomitantly installs a second useful functional group, such as halide, would be highly attractive and facilitate access to more complex materials with desirable properties.

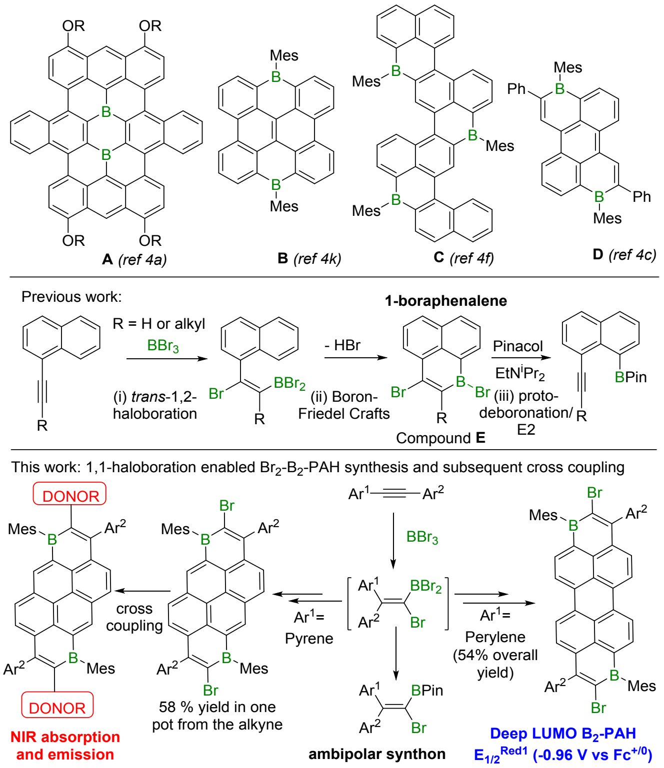

Figure 1: Top, select example of some of the largest / lowest LUMO B_n-PAHs (n > 1) containing three coordinate C_3B units. Middle, previous work forming boraphenalenes by bromoboration / S_EAr. Bottom, this work accessing and utilising large, low LUMO energy dibrominated B_2-PAHs.

[a] EaStCHEM School of Chemistry, University of Edinburgh, Edinburgh, EH9 3FJ, UK
[b] School of Chemistry, University of Manchester, Manchester, M13 9PL, UK
[c] Organic Semiconductor Centre, EaStCHEM School of Chemistry, University of St Andrews, St Andrews, KY16 9ST, UK
Corresponding author: michael.ingleson@ed.ac.uk

Electronic Supplementary Information (ESI) available: full experimental details, NMR spectra, crystallographic data, optoelectronic data and Cartesian coordinates for all calculations. See DOI: 10.1039/x0xx00000x

View Article Online
DOI: 10.1039/C9SC05404A

In our previous work, a one-pot synthesis of 1-boraphenalenes via sequential bromoboration / intramolecular boron-Friedel-Crafts of 1-alkynylnaphthalenes (Fig. 1, middle) was described.[7] We envisaged that this methodology could be extended by: (i) using larger (than naphthalene) π-scaffolds to obtain B_1 and B_2 doped PAHs possessing deeper LUMOs; (ii) utilising the bromo substituent to access more complex materials with desirable properties via coupling reactions. Herein these two objectives are realised enabling access to the lowest LUMO energy ambient stable B_n-doped PAH reported to date, to the best of our knowledge, and a low-optical gap D-A-D material where the acceptor unit is a B_2-PAH. In addition, mechanistic studies on the bromoboration/S_EAr process revealed it proceeds by alkyne 1,1-bromoboration, a process not previously observed. Therefore 1,1-bromoboration also was applied to simple diarylalkynes demonstrating its utility for forming 1-bromo-2,2-diaryl substituted vinylboronate esters that are otherwise challenging to access.

Results and Discussion

Synthesis of boron-doped PAHs and 1,1-bromoboration studies

Initially, 1-(pent-1-yn-1-yl)pyrene, **1**, was combined with BBr_3 in the presence of one equivalent of 2,4,6-tri-*tert*-butylpyridine (TBP), targeting an analogous *trans*-haloboration / S_EAr process that previously afforded 1-boraphenalenes.[7] Post protection at boron by reaction with dimesitylzinc, purification afforded two isomeric compounds, **1a** and **1b** (Scheme 1) in low yield, partly due to low stability of these compounds to the column chromatography. To provide enhanced stability, the bulkier 2,4,6-tri*iso*propylphenyl (Tip) protecting group was used instead of mesityl (Mes). Using similar reaction conditions, compounds **1c** and **1d** were isolated in higher yields relative to **1a** and **1b**.

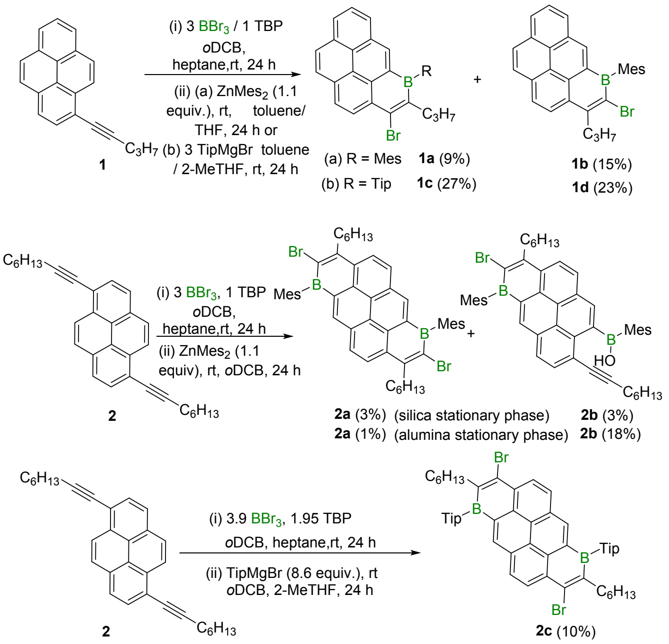

Scheme 1: Isolated products from the reaction of alkyl-alkynyl-pyrenes with BBr_3.

B_2-doped PAHs were next targeted through a two-fold bromoboration/S_EAr sequence starting from 1,6-di(pent-1-yn-1-yl)pyrene, **2**. However, post borylation/protection at boron, compound **2a** was the only fully fused B_2-PAH isolable via column chromatography in our hands and it was obtained in a very low yield alongside **2b**. Compound **2b** presumably derives from protodeboronation of a vinyl C-B unit (analogous to that in **1a**) followed by an E2 elimination reaction as previously observed for the 1-boraphenalenes (see figure 1, middle right).[7] Tip installation conditions also were applied to the product mixture derived from BBr_3 / **2**, however this led to the formation of compound **2c** in 10% yield as the only isolable product in our hands. The structures of **1a**, **2a** and **2c** were confirmed by single crystal X-ray diffraction analysis (see subsequent discussion). It should be noted that products derived from both 1,2 and 1,1-haloboration were observed (e.g. the B-Br analogues of **2a** / **2c**) and this may explain the complex mixtures observed starting from **2** with lower symmetry (than **2a**/**2c**) borylated products also observed spectroscopically (presumably containing one 1,1 and one 1,2-bromoborated boracycle in the same molecule).

In previous work 1-(arylethynyl)naphthalenes reacted with BBr_3 to give different products to that starting from 1-(alkyl-ethynyl)naphthalenes, with the former affording products from a 1,1-bromoboration/S_EAr cyclisation process (e.g. **F,** inset scheme 2, is formed instead of an analogue of **E**, Figure 1 middle),[7] with no 1,2-bromoboration derived products observed. Therefore, aryl-alkynyl-pyrene derivatives (e.g. **3**) were utilised in an attempt to avoid forming mixtures derived from competing 1,1 and 1,2-bromoboration. Starting from **3**, the desired Tip protected product **3a** was isolated in 75% yield with negligible 1,2-bromoboration products observed. In addition, the borinic acid **3b** was accessible in good yield using simple aqueous workup conditions. **3b** proved sufficiently stable for column chromatography and even survived 1 M HCl (aq.) for at least 0.5 h. Notably, all the aryl-substituted derivatives studied herein proved more resistant to protodeboronation than the alkyl congeners, with protection by mesityl also providing sufficient stabilisation for these derivatives. The NMR data for **3a**/**3b** are comparable to that previously reported for the B-OH and B-aryl 1-boraphenalenes.[7]

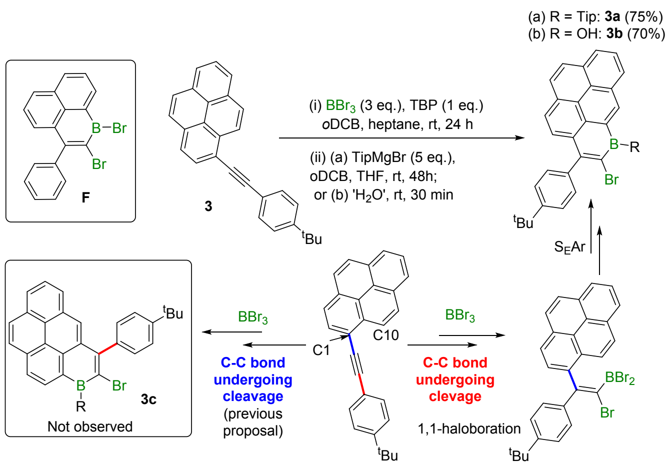

Scheme 2: Formation of **3a** and **3b** and mechanistic implications.

View Article Online
DOI: 10.1039/C9SC05404A

Earlier studies on the bromoboration of diphenylacetylene using BBr_3 by Lappert and co-workers suggested that only the 1,2-*cis*-bromoboration product (**4**, Scheme 3 inset) forms.[8] Furthermore, alkyne 1,1-haloboration using boron electrophiles was to the best of our knowledge unprecedented prior to this work, with 1,2-haloboration or 1,1-carboboration the general outcomes.[9] Thus, in our previous report on the bromoboration of 1-(arylalkynyl)-naphthalenes,[7] a mechanism was proposed for forming **F** that avoided 1,1-bromoboration. According to that previously proposed mechanism, compound **3c** (inset Scheme 2) should be obtained starting from **3** via cleavage of the pyrene C1-C_{alkyne} bond. However, X-ray diffraction analysis of the haloboration products **3a** and **3b** confirmed that boron was attached to C10 of pyrene and that the C1-C_{alkyne} bond remains intact. These observations indicate the reaction most likely proceeds through 1,1-bromoboration followed by electrophilic C-H borylation (Scheme 2, bottom right). Therefore, the bromoboration of other diarylalkynes, including diphenylacetylene, using BBr_3 was revisited to probe the apparent discrepancy with earlier work.

On combining diphenylacetylene with BBr_3 in heptane, crystals precipitated over the course of 5 mins. X-ray diffraction analysis on these revealed them to be the 1,2-*cis*-bromoboration product, **4** (inset scheme 3). NMR studies under the same conditions revealed that only one product is observed in solution, assigned as compound **4**. Protodeboronation of this reaction mixture afforded 1-bromo-1,2-diphenylethene, **4-H** with no 1,1-bromoboration isomer (**5-H**, Scheme 3) observed. While these observations are consistent with previous work,[8] upon heating the reaction mixture in heptane at 60 °C an additional product, assigned as **5**, was observed (by $^{13}C\{^{1}H\}$ and ^{11}B NMR spectroscopy). Protodeboronation of this reaction mixture afforded 1-bromo-2,2-diphenylethene, **5-H**, derived from 1,1-haloboration as the major product along with minor amounts of 1-bromo-1,2-diphenylethene (**4-H**). Notably, when bromoboration was performed in DCM, both 1,2- and 1,1-bromoboration products were observed after short reaction times at 20 °C (ca. 10 minutes by NMR spectroscopy and by analysis of products post protodeboronation). These observations suggest that 1,1-bromoboration proceeds through a polar transition state(s), and potentially a vinyl cation type intermediate(s), more stabilised by the polar solvent DCM. Identical product distributions also were observed using 3 equiv. of BBr_3 in place of 1.5 equiv. of BBr_3.

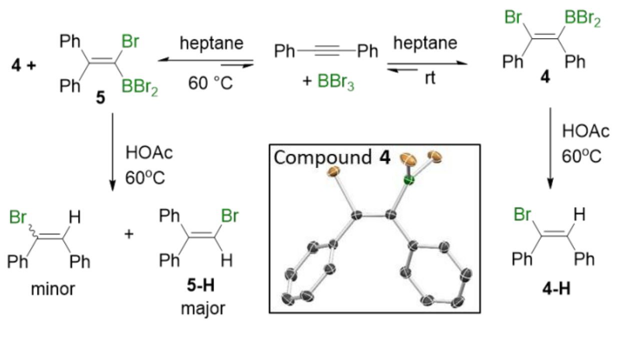

Scheme 3: The observation of 1,1- and 1,2-bromoboration under different conditions. Inset, the solid state structure of **4**, hydrogens omitted for clarity.

Similar outcomes were observed with di-*p*-tolylacetylene (**6**) and 1,2-bis(4-fluorophenyl)ethyne with the 1,1-haloboration product being the major species observed in DCM in both cases. Exact ratios of the BBr_2 1,1 : 1,2-haloboration (both cis and trans isomers) products in DCM are challenging to determine in-situ by NMR spectroscopy due to uncertainty in isomer assignment. Furthermore, ratios of BPin/vinyl C-H products post work-up and isolation are not indicative of *in-situ* ratios due to competing pinacol protection / protodeboronation / retrohaloboration (see Supporting Information section 4 for further discussion). For di-*p*-tolylacetylene a mixture of bromoboration products (ca. 3:10) was formed in DCM 10 minutes after the addition of BBr_3 at room temperature. To determine the identity of the major isomer the fact that alkyne 1,2-bromoboration products (e.g. **4**) are converted rapidly back into the starting alkyne on adding pyridine,[8] (concomitantly forming pyridine-BBr_3) was exploited. Upon addition of pyridine to the 3:10 bromoboration reaction mixture, the minor bromoboration product, assigned as **6a** (Scheme 4), was converted into the starting alkyne and pyridine-BBr_3, while the major bromoboration product, assigned as **6b**, formed an adduct, **7**, with pyridine at room temperature. Upon heating at 60 °C, compound **7** also converted into di-*p*-tolylacetylene and pyridine-BBr_3. Addition of excess BBr_3 to the mixture containing **7** to sequester all pyridine as pyridine-BBr_3 regenerated the mixture of 1,2- and 1,1-haloboration products in an identical 3:10 ratio to that originally observed. Combined these results indicate that 1,1-haloboration dominates in DCM, that this reaction reaches its equilibrium position rapidly in DCM, and that both 1,2- and 1,1-bromoboration are reversible. DFT calculations (at the M06-2X/6-311G(d,p) PCM (DCM) level) revealed the 1,1- and 1,2-bromoboration products (e.g. **4** and **5**) were effectively isoenergetic (all pairs of isomers had $\Delta E < 1.3$ and $\Delta G < 0.8$ kcal mol^{-1}) consistent with the observation of mixtures on reaching equilibrium. Finally, 1,1-bromoboration is not limited to diarylalkynes, with 1-phenyl-1-propyne also leading to 1,1-bromoboration products.

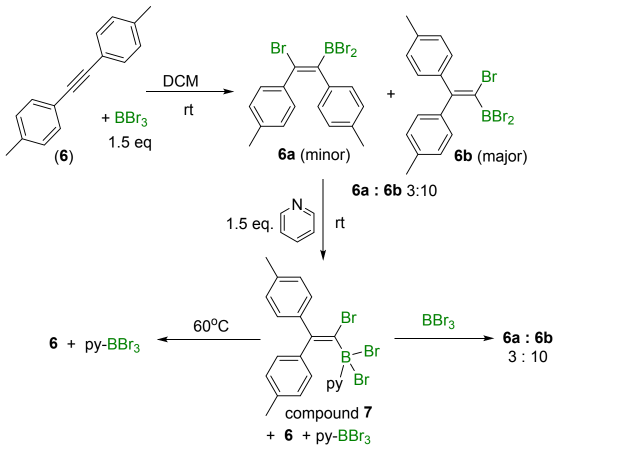

Scheme 4: Bromoboration in DCM, and reactivity of products towards pyridine.

The preparation of fully-substituted 1-bromo-1-alkenyl boronate esters currently is challenging (the major route to these types of compounds proceeds via hydroboration of alkynyl-halides thus is limited to forming tri-substituted

View Article Online
DOI: 10.1039/C9SC05404A

alkenes).[10] Indeed diaryl-derivatives (such as **8a-f** Scheme 5), have not been previously reported to the best of our knowledge. While 1,1-bromoboration represents a simple approach to these compounds to be useful protection at boron without (or with minimal) competing formation of the starting alkyne by retro-bromoboration is required. In the presence of excess triethylamine, the 1,1-bromoboration products (e.g. **5**)

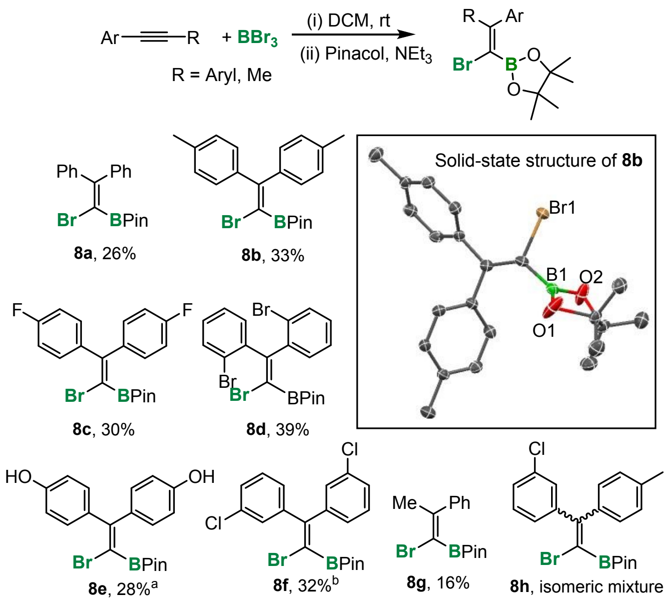

Scheme 5: 1,1-haloboration and pinacol protection with yields. Inset right, solid state structure of **8b**, hydrogens omitted for clarity, ellipsoids at 50% probability. A = from the p-MeO derivative with ether cleavage occurring concomitantly to haloboration. B = pinacol protected without Et_3N.

were converted into the pinacol boronate esters, **8a-g** demonstrating that ortho, meta and para substituted aryl-alkynes are amenable to this procedure. The yields are moderate at best due to the presence of the 1,2-isomer in the reaction mixture and the propensity of the Br-vinyl-BBr_2 isomers (e.g. **4** and **5**) to undergo retrohaloboration in competition to pinacol protection (see supporting information for more details). Indeed, under these conditions all the 1,2-bromoboration products (and the mass balance of the 1,1-haloboration products) were converted into the starting alkyne and Et_3N-BBr_3. Attempts at pinacol installation in the absence of base led to competitive protodeboronation (presumably due to the HBr by-product from pinacol installation onto the BBr_2 moiety) and lower yields of **8x** in most cases. The pinacol boronate esters were fully characterised and a number confirmed by X-ray diffraction analysis (e.g. inset scheme 5). It should be noted that substrates containing CF_3 were not amenable to this process due to B-F/C-Br bond formation on addition of BBr_3. Furthermore, ether cleavage occurs concomitantly to haloboration, with substrate **8f** isolated from the 4-methoxyaryl precursor. In addition, attempts to bromoborate 2,2'-bisthienylethyne with BBr_3 were successful to some extent, but protection with pinacol under a range of conditions was unsuccessful. This instead led to protodeboronation under a range of conditions. Finally an electronically biased diaryl alkyne was subjected to haloboration in DCM, however pinacol protection revealed that multiple haloborated isomers, e.g. **8h**, had formed that could not be separated in our hands.

With an understanding of the bromoboration process in hand, the extension of 1,1-haloboration/S_EAr to other substrates was explored. Using 1,6-bis((4-(*tert*-butyl)phenyl)ethynyl)pyrene, **9** (an analogue of **2**) and BBr_3 this sequential transformation worked effectively and post mesityl installation afforded **9a** in 58% yield in a one-pot reaction staring from **9**. Compound **9a** proved bench stable (as **9-12 a/b** all are) and was purified via column chromatography. The borinic acid **9b** could also be prepared from **9** in 62% yield via a simple hydrolytic work-up. Starting from 7-(*tert*-butyl)-1,3-bis((4-(*tert*-butyl)phenyl)-ethynyl)pyrene, **10**, both the Mes-protected product **10a** and the borinic acid **10b** also were accessible, albeit isolated in lower yields. 1,1-haloboration/S_EAr also was applicable to perylene substrates. For 3-(*p*-tolylethynyl)perylene, **11**, the Tip-protected product **11a** (50%) and the borinic acid **11b** (88%) were isolated post column chromatography. The bromoboration/S_EAr cyclisation reaction also worked with 3,9-bis((4-(*tert*-butyl)phenyl)ethynyl)perylene, **12**, to yield the Mes-protected compound B_2-PAH **12a** (54% yield) and the borinic acid **12b** (82% yield) depending on the protection protocol.

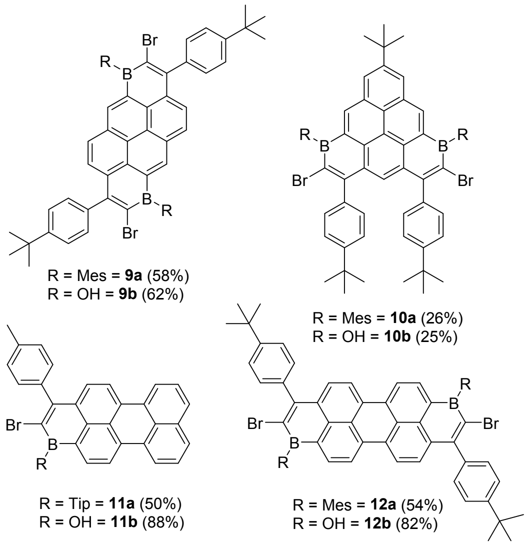

Scheme 6: The formation of extended B_n-PAHs by bromoboration/S_EAr.

Solid-State Structures:

The solid-state structures of B_1-PAHs **1a**, **1c** and **3b** revealed effectively planar six-membered boracycles with boron atoms adopting a trigonal planar geometry (Σ(C-B-C) ≈ 360°). Notably, the C12-C13 bond length (1.355(5) Å in **1a**) is shorter than the C11-C12, C1-C10 and C10-C11 bond lengths (1.462(5), 1.448(5) and 1.414(4) Å, respectively in **1a**) as is the case in **1c** and **3b**. The bond length alternation indicates the lack of significant π delocalisation within the boracycle as was observed with the 1-boraphenalenes.[7] The fusion of a boracycle onto the PAH core does have some impact, for example on the C-C bond in the K-region of pyrene. For **1a** the bond length of C1-C2 (1.367(4) Å) is longer than that of C14-C15 (1.337(5) Å). The elongation of

View Article Online
DOI: 10.1039/C9SC05404A

C1-C2 Vs C14-C15 may indicate some delocalisation of this π-electron density into the boron centre.[11a] For compound **3b**, the B-O bond length (1.369(4) Å) is close to the reported values for other related borinic acids, indicating some multiple bond character between boron and oxygen. The Mes/Tip and *tert*-butylphenyl groups are all almost orthogonal to the boracycle, which precludes close face to face pi stacking involving the boracycles in the intermolecular structure.

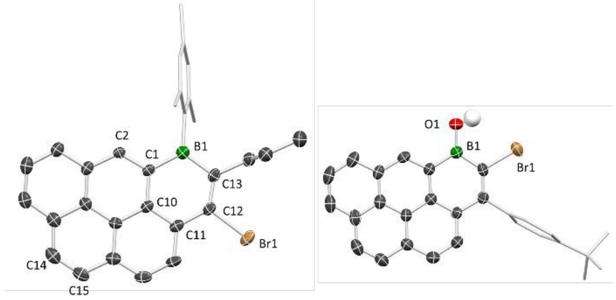

Figure 2: Solid-state structures of **1a** (left) and **3b** (right), most hydrogens omitted for clarity. Ellipsoids at the 50% probability level.

The solid-state structures of the B_2-doped PAHs **2a**, **2c**, **9a, 10b** and **12a** also were determined (Figures 3-4 and SI). All five compounds show planar π-conjugated cores with the peripheral substituents effectively orthogonal to the PAH core. As a result, no face to face π-stacking is observed in the extended structures for these compounds (excluding **10b**, see SI). For example, the face to face intermolecular separation of the cores of two parallel molecules is found to be 6.67 Å for **2c**. The boracycle metrics are similar to the mono-borylated compounds with C-C bond length alternation within the boracycles also observed (for example a C11-C12 vinylic distance in **12a** of 1.359(7) Å and long endocyclic B-C bonds 1.534(6) and 1.543(6) Å indicate minimal π delocalisation consistent with previous NICS calculations).[7] Notably, for the diborylated pyrene compounds, the length of the C-C bonds in the pyrene K-region is longer than that in mono-borylated compound (e.g. the bond length of C7-C10 is 1.379(3) Å for compound **2c**). The elongation of C7-C10 bond length may indicate a greater delocalisation of these π-electrons into the boron centres for the di-borylated compounds relative to the mono-borylated compounds.

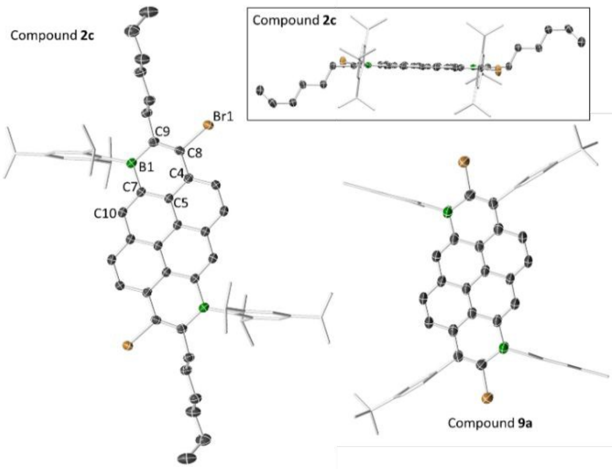

Figure 3: Solid state structures of **2c** (two views) and **9a**, with hydrogens omitted for clarity. Ellipsoids are at the 50% probability level.

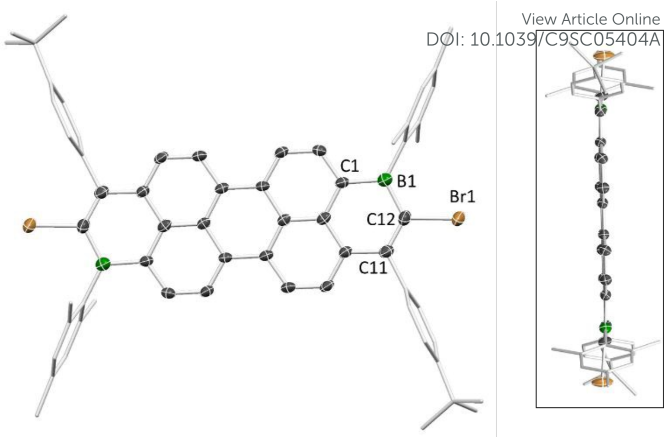

Figure 4: Solid state structure of **12a** (two views), with hydrogens omitted for clarity. Ellipsoids are at the 50% probability level.

Cyclic voltammetry:

The first reduction potentials ranged from -1.91 V (**3b**) to -0.96 V (**12a**, table 1). Within the scan window, the B_1-doped PAHs showed one reversible reduction wave except for compound **11a**, for which two reduction waves were observed. All B_2-PAHs showed two reversible reduction waves; however, no oxidation waves were observed within the solvent window for these compounds. The hydroxyl group on boron reduced the electron-accepting abilities of the boron-doped PAHs compared with the Tip/Mes group as previously observed.[4c] Also as noted by Würthner and co-workers,[4c] the boron doping pattern also significantly influences the redox properties with the first reduction potential of **9a** more positive than that of **10a** by 0.15 V (for **9b** vs **10b** $\Delta E_{1/2}^{red1}$ = 0.32 V). Notably, the reduction potential of **9a** is more positive than bis-($BMes_2$)-pyrenes (4,9 isomer $E_{1/2}^{red1}$ = -2.31 V, 1,6 isomer $E_{1/2}^{red1}$ = -1.81 V)[11] and the products from the electrophilic borylation of 1,6-(2-pyridyl)$_2$-pyrene (when the boron moiety = BPh_2 $E_{1/2}^{red1}$ = -2.08 V)[14] this is ascribed to greater π delocalization in **9a** as a result of planarization and three-coordinate B centres. Finally, **9a** has a much more positive reduction potential than its all carbon analogue (for which $E_{1/2}^{red1}$ = -2.11 V),[15] further confirming boron-doping as an effective strategy to obtain molecules with deep LUMOs due to their electron-deficient nature (B_2-PAHs are isoelectronic to dicationic carbon analogues).

Comparing pyrene and perylene core structures the reduction potentials of the borylated perylene compounds are positively shifted relative to the pyrene substrates. For example, the monoborylated compound **11a** exhibited the first reduction wave at -1.43 V more positive than **3a** by 0.23 V. Indeed among all the compounds investigated, **12a** shows the least negative first reduction potential with $E_{1/2}^{red1}$ = -0.96 V, which is also much more positive than the related all carbon peropyrenes.[16] To the best of our knowledge, compound **12a** has the least negative reduction potential of all ambient stable three coordinate at boron B-doped PAHs reported to date, with compound **D** being the ambient stable B_n-PAH with the next least negative reduction potential (table 1).[4c]

View Article Online
DOI: 10.1039/C9SC05404A

Table 1: Optoelectronic properties of B_n-PAH compounds and a PDI for comparison

	$E_{1/2}^{red1}$ (V)[a]	$E_{1/2}^{red2}$ (V)[a]	$LUMO^{exp}$ (eV)[b]	λ_{abs} [ε / 10^{-3} M^{-1} cm^{-1}] (nm)[c]	λ_{PL} (nm)[c]	Φ_{PL} (%)[d]	E_g (eV)[e]	HOMO (eV)[f]	LUMO (eV)[f]
3a	-1.66	-	-3.49	375 [18.04], 395 [15.12], 417[13.16], 491[17.98]	553, 592	9.2	2.26	-7.04	-2.29
3b	-1.91	-	-3.24	359[3.81], 383[3.62], 404[5.34], 449[7.86]	500, 532	8.7	2.51	-6.97	-2.05
9a	-1.03	-1.49	-4.12	345[3.23], 362[4.74], 396[2.64], 536[24.13], 567[18.00]	599, 648	2.0	2.07	-7.26	-2.98
9b	-1.42	-1.73	-3.73	340[2.41], 355[3.69], 390[1.56], 501[32.13],528[25.05]	557, 598	6.8	2.23	-6.97	-2.60
10a	-1.30	-2.11	-3.85	332[20.75], 386[21.72], 406[35.98], 435[15.45], 508[3.64], 545[4.88], 588[3.52]	614, 668, 729	5.9	2.00	-7.19	-2.67
10b	-1.61	-2.25	-3.54	380[34.50], 417[3.93], 443[6.04], 476[8.37], 507[11.57], 543[8.22]	560, 605, 657	46.9	2.19	-7.00	-2.43
11a	-1.43	-2.06	-3.72	314[57.13], 360[8.01], 405[10.53], 431[15.93], 456[26.37], 500[16.68], 534[33.55], 573[43.71]	591, 628	0.6	2.08	-6.76	-2.50
11b	-1.57	-	-3.58	312[28.42], 340[5.37], 410[7.71], 433[14.85], 456[13.10], 487[29.85],521[31.05]	532, 570, 618	0.4	2.31	-6.68	-2.29
12a	-0.96	-1.28	-4.19	336[5.91], 392[5.49], 528[18.02], 568[44.48], 614[68.41]	634, 686	1.6	1.93	-7.06	-3.08
12b	-1.28	-1.54	-3.87	370[1.48], 494[4.90], 530[12.52], 571[19.61]	582, 630	3.8	2.10	-6.86	-2.74
D[g]	-1.07	-1.41	-4.08	611, 417	668	74		-	-
PDI[h]	-1.02		-4.13	527	534	99		-7.21	-2.89

a = Measurements carried out at 298 K in THF with 0.1 M $^nBu_4NPF_6$ as the supporting electrolyte. Electrochemical reduction potentials were calibrated with ferrocene as internal standard and referenced vs Fc^+/Fc. b = $E_{LUMO} = -E_{1/2}^{red} - 5.15$ eV.[12] c = Optical measurements carried out at 298 K in toluene at 1×10^{-5} M. d Under aerated conditions using $[Ru(bpy)_3](PF_6)_2$ in CH_3CN as the reference (Φ_{PL}: 1.8%). e = E_g were determined at the energy corresponding to 10% of the lowest energy absorption band. f = from calculations at the M06-2X/6-311G(d,p) level. g = from ref. 4c. h = PDI refers to the perylene diimide with N-DIP substituents from ref. 13.

Photophysical properties:

By varying the polycyclic core and the boron substituent, a series of B_n-doped PAHs (n= 1, 2) are obtained forming solutions with colours ranging from yellow to dark blue. UV-vis absorption and fluorescence spectra were recorded and the optical energy gap estimated (Table 1). All compounds showed well resolved absorption/emission profiles with small Stokes shifts. Consistent with the observed solution colours, the obtained spectra showed the lowest energy absorption band spanning 449 nm (**3b**, light yellow solution) to 614 nm (**12a**, dark blue solution). The double borylated compound **9a** showed λ_{max} at 567 nm, which is red-shifted by 82 nm compared with the mono-borylated compound **3a** (λ_{max} = 491 nm). The same trend was also observed for **11a**/**12a**, due to the extended conjugation and double boracycle annulation leading to narrower HOMO-LUMO gaps. In addition, all borinic acids exhibited hypsochromic shifts of their lowest absorption band by ca. 40 nm compared with the Tip/Mes protected analogues. The photoluminescence quantum yield (Φ_{PL}) of the brominated compounds studied herein were relatively low, which might be attributed to the heavy atom effect of bromine, as related heavy atom free analogues reported by Würthner and co-workers are notably more emissive (Φ_{PL}s up to 95%).[4c]

Computational studies

To provide more insight into the trends observed in the experimental data, DFT calculations were performed at the M06-2X/6-311G(d,p) level with a polarisable continuum model (PCM) of DCM, calculations for emulated the full compound (except for **2c**, see SI). The trend in the LUMO energies from the computational results were consistent with the trends in the cyclic voltammetry data with compound **3b**, that has the most negative reduction potential, being calculated to have the highest LUMO energy (-2.05 eV) among the compounds studied, while compound **12a** with the least negative reduction potential was predicted to have the deepest LUMO level (-3.08 eV, see Figure 5). It is noteworthy that the computed LUMO energy level of **12a** is lower than that of a perylene diimide (PDI, in red Figure 5) calculated at the same level of theory. Indeed comparison of the CV data for **12a** and a PDI compound (containing all C-H and two N-DIP groups), confirms that **12a** has the deeper LUMO,[13] while **9a** has very similar frontier orbital energies to this PDI (Table 1). This further indicates that both these diborylated pyrene and perylene compounds have potential as acceptor moieties in organic electronics.

View Article Online
DOI: 10.1039/C9SC05404A

Figure 5: Calculated frontier orbitals (shown at iso-values of 0.03) for several B_2-PAHs and for comparison an N-Me substituted PDI. Ar = *p*-^{t}Bu-phenyl.

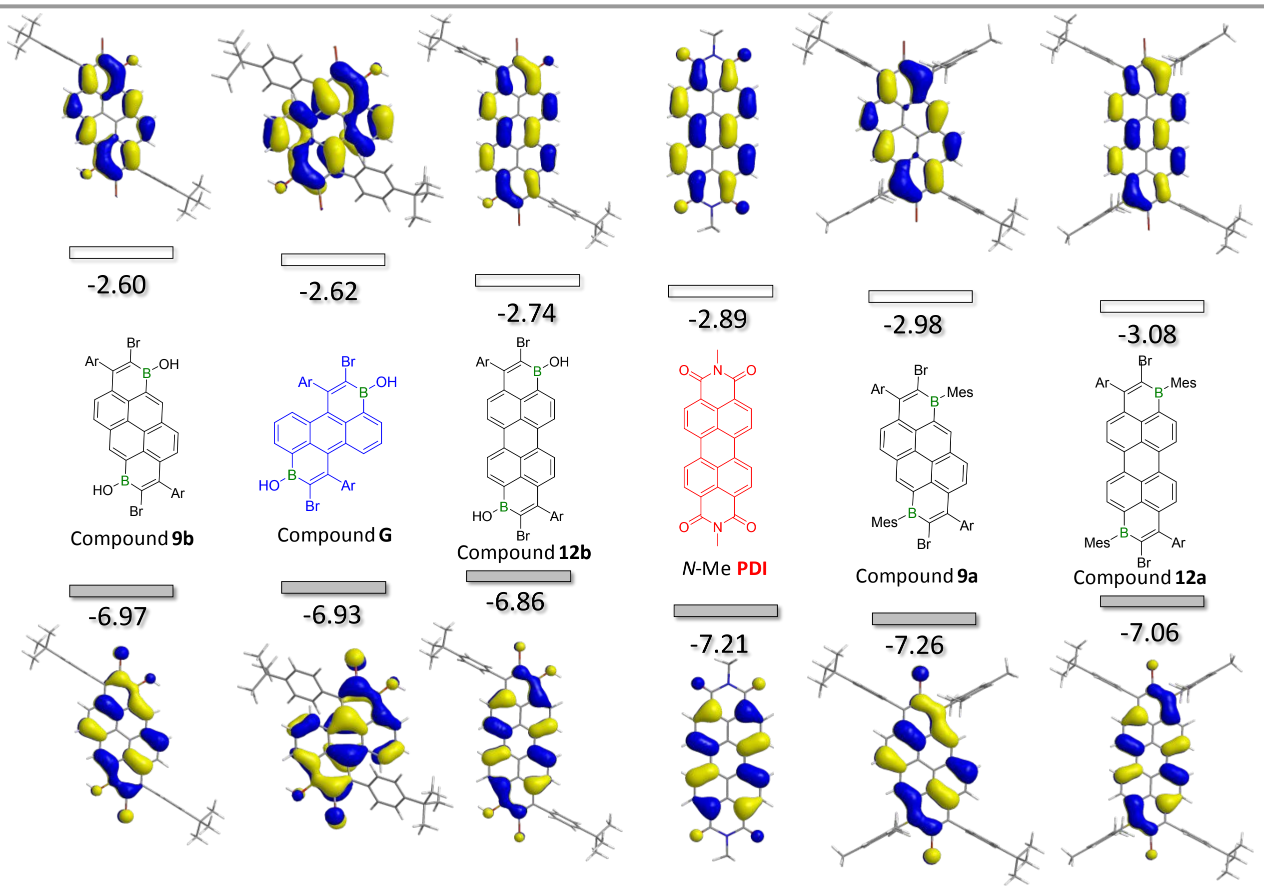

As shown in Figure 5 and the SI, the LUMO and HOMO of all molecules are delocalised over the whole π-backbone and involve boron contributions to both. Interestingly, the frontier molecular orbital distributions of **12a** and **12b** are very similar to that of PDI. Furthermore, the frontier orbitals of all the B_2-PAHs studied herein (and indeed the related compounds reported by Würthner et al.)[4c] are related closely to the calculated HOMO and LUMO of the parent π core molecule (e.g. the HOMO and LUMO of pyrene and perylene)[17] with some additional contributions from the appended B-C unit. For completeness, the anthracene-based compound **G** (blue, Figure 5) was also calculated, which revealed that the HOMO and LUMO of this compound also was related in character to the HOMO and LUMO of anthracene. Note, attempts to synthesise **G** failed in our hands, possibly due to the additional peri C-H group inducing steric clash with the proximal aryl group (with some structural distortion observed in the calculated structure of **G**). It is notable that the trend in the relative HOMO/LUMO energy and optical gap of **9b**, **G** and **12b** mirrors that of the parent PAH core,[18] with perylene (deepest LUMO / highest HOMO) < anthracene < pyrene (highest LUMO / deepest HOMO) for optical gap. This indicates that access to even lower LUMO energy B_2-PAHs for this series maybe possible starting from lower energy LUMO core PAH structures.

Functionalisation of Boron Doped PAHs by Cross Coupling

One attraction of the compounds reported herein is the potential utility of the bromide unit, derived from the concomitant installation of B/Br in the initial step of Bn-PAH formation. While cross coupling reactions can be performed using the C-B units as the nucleophilic coupling partner,[19] this removes the electronic effect of B-doping, thus utilising the C-Br unit in cross-coupling reactions offers a way to construct complex functional electronic materials that retain the C_3B units that impart the deep LUMO character.[3] Initially compound **3a** containing the sterically more demanding Tip unit, was explored and found to be amenable to Negishi cross coupling reaction conditions. Specifically, in the presence of $Pd(PPh_3)_4$, **3a** reacted with the in-situ generated aryl-zinc reagent affording the desired product **13** (Scheme 7) in moderate 33% isolated yield. We attribute the modest yield to the highly sterically encumbered vinyl-Br position present in these B-PAHs, thus the B-Mes derivatives were explored.

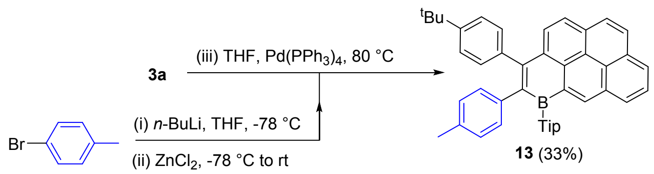

Scheme 7: Negishi cross coupling to form compound **13**.

View Article Online
DOI: 10.1039/C9SC05404A

The same methodology could be applied to B-Mes derivatives to access a D-A-D molecule with a narrow HOMO-LUMO energy gap. Using the procedure established for **13**, **9a** was coupled with the organozinc compound derived *in-situ* from 4-bromotriphenylamine to construct compound **14** (Figure 6). The desired double cross coupled product, **14**, was isolated by column chromatography in 21% yield. Cyclic voltammetry measurements on compound **14** showed one oxidation wave within the solvent window (peak-current E_{ox} = 0.49 V vs Fc/Fc$^+$) and two reduction processes ($E_{1/2}^{red1}$ = -1.23 V, $E_{1/2}^{red2}$ = -1.62 V). The first reduction process is shifted cathodically by 0.2 V relative to **9a**, presumably due to the replacement of inductively electron-withdrawing bromine for the triphenylamine groups. DFT calculations (Fig. 6, bottom) were performed on compound **14** at a lower level due to its size (M06-2x/6-31G(d)), **9a** was calculated at the same level for direct comparison (which confirmed effectively identical HOMO/LUMO distributions for **9a** using the two basis sets). Consistent with a D-A molecule the HOMO/LUMO are spatially separated, with the HOMO predominantly localised on the triaryl amine unit thus being 0.91 eV higher in energy than the HOMO of **9a**. The LUMO in **14** is localised on the B_2-PAH acceptor unit and is closely related in character to the LUMO of **9a**. Notably, the calculated energy for the LUMO of **14** is 0.19 eV higher than that for **9a** in excellent agreement with the CV data; again this is attributed to the exchange of inductively withdrawing Br groups for triarylamine units.

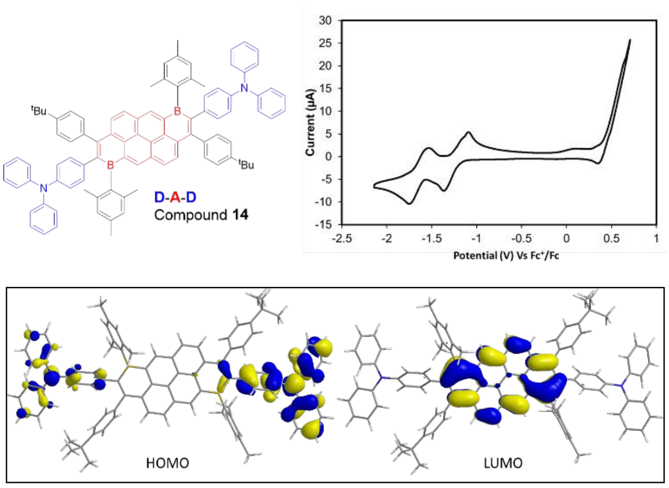

Figure 6: CV data, for compound **14** (1 mM solution in THF with 0.1 M $[NBu_4][PF_6]$, potential calibrated Vs Fc/Fc$^+$). Inset bottom, HOMO and LUMO of compound **14** (isovalue 0.025) at the M06-2x/6-31G(d) level.

The photophysical properties of **14** in solution, solid-state and dispersed in a PMMA film were investigated. Compound **14** displayed a broad absorption band stretching up to 750 nm in dichloromethane, with the onset corresponding to a optical gap of 1.65 eV (comparable to ΔE_{redox} determined by electrochemistry). Thus, the strong acceptor character of the B_2-PAH unit combined with the triphenylamine donor units results in a low HOMO-LUMO energy gap. We employed time-dependent DFT (TDDFT) calculations using the Tamm-Dancoff approximation at the PBE0/6-31G(d,p) level of theory to assign the spectral features observed in the absorption spectrum of **14**. The lowest energy absorption features found within the tail of the band showing a maximum at 530 nm and a shoulder at 600 nm are assigned to be charge transfer (CT) states from the Ph_2NPh group to the B_2-PAH core ($S_0 \rightarrow S_1$, $S_0 \rightarrow S_2$). The principal distinguishable absorption features at 444 nm originate from mixed CT/LE (LE = locally excited) transitions, but this time the CT contribution implicates the mesityl groups as donors to the B_2-PAH core ($S_0 \rightarrow S_3$, $S_0 \rightarrow S_4$, see supporting information for more details); the LE contribution is localized on the B_2-PAH acceptor. Higher energy bands involve increasing contributions of LE transitions of the B_2-PAH core. Recognizing the propensity of large acenes to aggregate in solution, even at very dilute concentrations we next investigated the effect of concentration on both the absorption and emission spectra. We note that both the ε values and the spectral features were independent of concentration, precluding aggregation of the molecule in its ground state in DCM at the concentrations studied (see Supporting Information). In contrast, the emission in DCM was highly concentration dependent. At 0.15 μmol/mL the emission is broad and unstructured and centred at 479 nm. As the concentration is increased to 63 μmol/mL, there is a decrease in intensity of this band coupled with a progressive and significant red-shift of the emission. At the highest concentrations studied, the emission narrows but remains unstructured (Figure 7). We attribute this complex behaviour to the formation of mixtures of different excimers as the concentration increases, presumably with higher order aggregates forming at the higher concentrations.

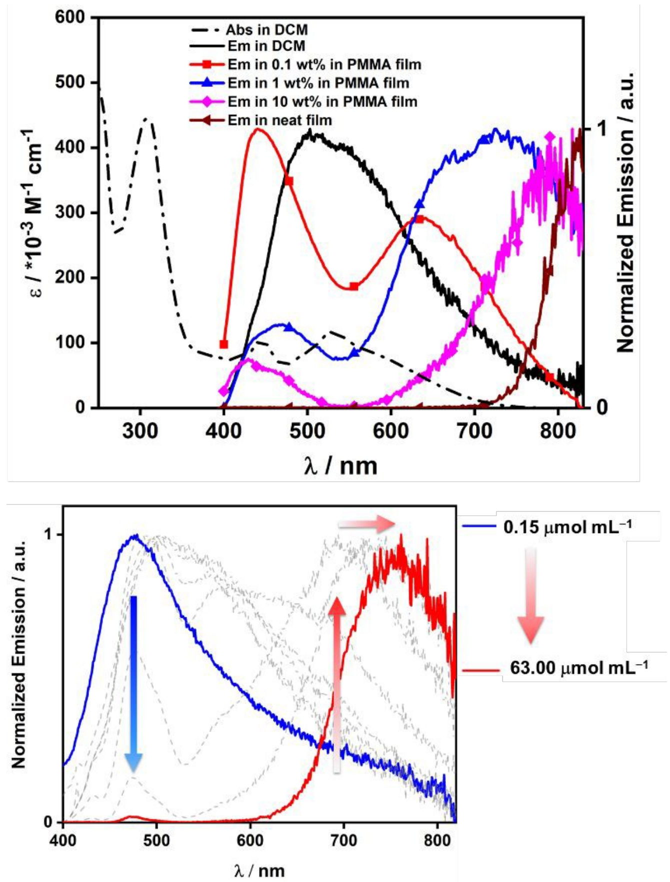

Figure 7: Top, photophysical data for compound **14** in DCM solution and in the solid state (neat film and dispersed in PMMA). Bottom, variation in the emission spectra on change of concentration of **14** in DCM solution. λ_{exc}=370 nm.

The Φ_{PL} value in DCM for **14** at 0.52 µmol mL^{-1} is 4% and this value is not sensitive to oxygen. The excited state emission decays measured at both dilute (0.52 µmol mL^{-1}) and concentrated (33 µmol mL^{-1}) solutions are multi-exponential in nature but remain in the ns regime, consistent with a fluorescence mechanism. In order to mitigate these non-radiative pathways, we next investigated the solid-state photophysical properties as thin films in PMMA at 0.1, 1 and 10 wt% doping concentrations, and as neat films. Generally, the same evolution in emission profiles is observed in the solid-state as was observed in DCM. As a 0.1 wt% PMMA doped film two unstructured emission bands are observed, one of higher relative intensity at high energy at λ_{PL} = 442 nm that we ascribe to the same monomer emission observed in dilute DCM, and a lower intensity and broader low energy band at λ_{PL} = 638 nm that we ascribe to excimeric emission. The Φ_{PL} of this film is 5%, which is essentially identical to that measured in DCM. This suggests that during the spin-coating process aggregation remains strong even at this low doping concentration. As a 1 wt% PMMA doped film, two unstructured emission bands remain, one at λ_{PL} = 472 nm and one at λ_{PL} = 726 nm; here, we note the large red-shift and significant enhancement in intensity of the low-energy band. The Φ_{PL} of this film is slightly lower at 3%. The 10 wt% doped PMMA film also shows two emission bands where the relative intensity of the high energy band at λ_{PL} = 434 nm is reduced further compared to the low energy band at λ_{PL} = 793 nm. The Φ_{PL} of this film is < 1%. The neat film shows only a single very weak and red-shifted emission band at λ_{PL} = 824 nm with a Φ_{PL} < 1%. There is a systematic shortening of the τ_{PL} with increasing doping concentrations that mirrors the decrease in Φ_{PL} (see Supporting Information). Irrespective of the complexity of the emission spectra the successful formation of the low optical gap material **14** demonstrates the utility of these dibrominated B_2-PAHs in accessing complex organic materials.

Conclusions

In conclusion, sequential bromoboration/ intramolecular electrophilic C-H borylation enables formation of a range of brominated B_n-doped PAHs in useful yields via an operationally simple, one-pot route from readily available precursors (alkynes and BBr_3). Cyclic voltammetry and photophysical studies revealed that these molecules have very low LUMO energies thus are attractive acceptor units for use in organic electronic applications. In particularly, compound **12a** has the least negative reduction potential among all reported ambient stable B-boron-doped PAHs to the best of our knowledge. The C-Br units in the B_n-PAHs can be utilised directly in Negishi cross-coupling reactions, which enabled formation of a donor-acceptor-donor molecule displaying solution absorption up to 750 nm. Finally, mechanistic studies on the bromoboration reaction indicated it proceeds through the 1,1-bromoboration of the diarylalkynes, a reaction not previously observed using just boron electrophiles. 1,1-Bromoboration can be applied to functionalise other diarylalkynes, enabling access to unprecedented 1-bromo-2,2-diaryl substituted vinylboronate esters direct from internal alkynes. The utility of the 1,1-bromoboration reaction is being studied further in our laboratory as are the brominated-B_2-PAHs, particularly to access useful functional materials.

Conflicts of interest

There are no conflicts to declare.

Acknowledgements

The research leading to these results has received funding from the European Research Council under the Horizon 2020 Research and Innovation Program (Grant no. 769599), the Leverhulme Trust (RPG-2014-340) and the EPSRC (EP/P010482/1). C. Si thanks the China Scholarship Council (201806890001). Dr G. Nichol is thanked for the collection of X-ray diffraction data, Dr G. Whitehead for the structure of **2a** and Dr A. Woodward for collecting photophysical data on compound **2c** (see Supporting Information).

Notes and references

1 Main Group Strategies towards Functional Hybrid Materials, ed. T. Baumgartner and F. Jäkle, John Wiley & Sons, Ltd., Chichester, 1st edn., 2018.

2 For recent reviews at least partly focused on PAHs containing C_3B units see: (a) Z. Huang, S. Wang, R. D. Dewhurst, N. V. Ignat'ev, M. Finze and H. Braunschweig, *Angew. Chem. Int. Ed.,* 2019, DOI: 10.1002/anie.201911108. (b) M. Hirai, N. Tanaka, Sakai and S. Yamaguchi, *Chem. Rev.*, 2019, **119**, 8291. (c) X.-Y. Wang, X. Yao, K. Müllen, *Sci. China Chem*., 2019, **62**, 1099 (d) S. K. Mellerup and S. Wang, *Trends in Chemistry*, 2019, **1**, 77; (e) E. von Grotthuss, A. John, T. Kaese and M. Wagner, *Asian J. Org. Chem*., 2018, **7**, 37; (f) M. Stepien, E. Gonka, M. Zyła and N. Sprutta, *Chem. Rev*., 2017, **117**, 3479; (g) L. Ji, S. Griesbeck and T. B. Marder, *Chem. Sci.*, 2017, **8**, 846; (h) A. Escande and M. J. Ingleson, *Chem. Commun*., 2015, **51**, 6257; (i) A. Wakamiya and S. Yamaguchi, *Bull. Chem. Soc. Jpn*., 2015, **88**, 1357. For their use in electrocatalysis see: (j) R. J. Kahan, W. Hirunpinyopas, J. Cid, M. J. Ingleson, R. A. W Dryfe, *Chem. Mater.* 2019, **31**, 1891.

3 For rare example of halogenated-B_n-PAH formation, in this case starting from halo-aromatic precursors and their utility in cross coupling, see: (a) C. Reus, S. Weidlich, M. Bolte, H.-W. Lerner and M. Wagner, *J. Am. Chem. Soc*., 2013, **135**, 12892; (b) A. Shuto, T. Kushida, T. Fukushima, H. Kaji and S. Yamaguchi, *Org. Lett.*, 2013, **15**, 6234.

4 For seminal work in the area of forming solely B_n-doped PAHs with three coordinate B centres see: (a) C. Dou, S. Saito, K. Matsuo, I. Hisaki and S. Yamaguchi, *Angew. Chem. Int. Ed.*, 2012, **51**, 12206; (b) Z. Zhou, A. Wakamiya, T. Kushida, S. Yamaguchi, *J. Am. Chem. Soc.,* 2012, **134**, 4529. For select recent examples on this topic see: (c) J. M. Farrell, C. Mützel, D. Bialas, M. Rudolf, K. Menekse, A.-M. Krause, M. Stolte and F. Würthner, *J. Am. Chem. Soc*., 2019, **141**, 9096. (d) J. Radtke, K. Schickedanz, M. Bamberg, L. Menduti, D. Schollmeyer, M. Bolte, H.-W. Lerner and Matthias Wagner, *Chem. Sci.,* 2019, **10**, 9017. (e) A. John, S. Kirschner, M. K. Fengel, M. Bolte, H.-W. Lerner and M. Wagner, *Dalton Trans*., 2019, **48**, 1871; (f) R. J. Kahan, D. L. Crossley, J. Cid, J. E. Radcliffe, A. W. Woodward, V. Fasano, S. Endres, G. F. S. Whitehead and M. J.

Ingleson *Chem. Commun*., 2018, **54**, 9490; (g) S. Kirschner, J.-M. Mewes, M. Bolte, H.-W. Lerner, A. Dreuw and M. Wagner, *Chem.–Eur. J*., 2017, **23**, 5104; (h) A. John, M. Bolte, H.-W. Lerner and M. Wagner, *Angew. Chem., Int. Ed*., 2017, **56**, 5588; (i) D. L. Crossley, R. J. Kahan, S. Endres, A. J. Warner, R. A. Smith, J. Cid, J. J. Dunsford, J. E. Jones, I. Vitorica-Yrezabal and M. J. Ingleson, Chem. Sci., 2017, 8, 7969; (j) J. M. Farrell, D. Schmidt, V. Grande and F. Würthner, *Angew. Chem., Int. Ed.,* 2017, **56**, 11846. (k) V. M. Hertz, M. Bolte, H.-W. Lerner and M. Wagner, *Angew. Chem. Int. Ed*., 2015, **54**, 8800.

5 There are also boron containing polymers that are B_n-PAHs with n>2, however, while chemically well-defined the value of n is not as they are polydisperse. For select examples see: (a) S. Kawai, S. Saito, S. Osumi, S. Yamaguchi, A. S. Foster, P. Spijker and E. Meyer, *Nat. Commun*., 2015, **6**, 8098; (b) R. R. Cloke, T. Marangoni, G. D. Nguyen, T. Joshi, D. J. Rizzo, C. Bronner, T. Cao, S. G. Louie, M. F. Crommie and F. R. Fischer, *J. Am. Chem. Soc*., 2015, **137**, 8872.

6 For examples of post synthetic modification of B_n-PAHs and subsequent functionalisation by cross coupling see: (a) T. Kushida, C. Camacho, A. Shuto, S. Irle, M. Muramatsu, T. Katayama, S. Ito, Y. Nagasawa, H. Miyasaka, E. Sakuda, N. Kitamura, Z. Zhou, A. Wakamiya and S. Yamaguchi, *Chem. Sci*., 2014, **5**,1296; (b) C. Hoffend, K. Schickedanz, M. Bolte, H.-W. Lerner, M. Wagner, *Tetrahedron*, 2013, **69**, 7073.

7 R. J. Kahan, D. L. Crossley, J. Cid, J. E. Radcliffe, M. J. Ingleson, *Angew. Chem. Int. Ed.*, 2018, **57**, 8084.

8 (a) M. F. Lappert, B. Prokai, *J. Organomet. Chem.* 1964, **1**, 384. (b) Related findings were subsequently published: J. J. Eisch, L. J. Gonsior, *J. Organomet. Chem.,* 1967, **8**, 53.

9 For recent studies combining alkynes and R_2B-X see: K. Skoch, C. Pauly, C. G. Daniliuc, K. Bergander, G. Kehr and G. Erker, *Dalton. Trans.* 2019, **48**, 4837; (b) J. R. Lawson, V. Fasano, J. Cid, I. Vitorica-Yrezabal and M. J. Ingleson, *Dalton Trans*., 2016, **45**, 6060. For an early example see: (c) R.-J. Binnewirtz, H. Klingenberger, R. Welte and P. Paetzold, *Chem. Ber*., 1983, **116**, 1271

10 In contrast tri-substituted 1,1-bromo-Bpin-alkenes derivatives are known, for a recent example see: Y. Pang, R. Kojima and H. Ito, *Org. Biomol. Chem*., 2018, **16**, 6187. For an early example see: H. C. Brown and T. Imai, *Organometallics*, 1984, **3**, 1392.

11 (a) L. Ji, I. Krummenacher, A. Friedrich, A. Lorbach, M. Haehnel, K. Edkins, H. Braunschweig, T. B. Marder, *J. Org. Chem.*, 2018, **83**, 3599. (b) S.-B. Zhao, P. Wucher, Z. M. Hudson, T. M. McCormick, X.-Y. Liu, S. Wang, X.-D. Feng, Z.-H. Lu, *Organometallics*, 2008, **27**, 6446.

12 Adapted from: C. M. Cardona, W. Li, A. E. Kaifer, D. Stockdale and G. C. Bazan, *Adv. Mater*. 2011, **23**, 2367.

13 A. Nowak-Krol, K. Shoyama, M. Stolete and F. Würthner, *Chem. Commun.,* 2018, **54**, 13763.

14 M. Vanga, R. A. Lalancette, F. Jäkle, *Chem. Eur. J.,* 2019, **25**, 10133.

15 Y. Gu, X. Wu, T. Y. Gopalakrishna, H. Phan and J. Wu, *Angew. Chem. Int. Ed.,* 2018, **57**, 6541.

16 W. Yang, R. R. Kazemi, N. Karunathilake, V. J. Catalano, M. A. Alpuche-Aviles and W. A. Chalifoux, *Org. Chem. Front.* 2018, **5**, 2288.

17 M. A. Filatov, S. Karuthedath, P. M. Polestshuk, S. Callaghan, K. J. Flanagan, T. Wiesner, F. Laquai, and Mathias O. Senge, *ChemPhotoChem*., 2018, **2**, 606.

18 A. P. Davis, A. J. Fry, *J. Phys. Chem. A.*, 2010, **114**, 12299.

19 (a) J. M. Farrell, V. Grande, D. Schmidt and F. Würthner, *Angew. Chem. Int. Ed.*, 2019, **58**, 16504. (b) E. Dimitrijevic, M. Cusimano and M. S. Taylor, *Org. Biomol. Chem.* 2014, **12**, 1391.